*J. Fluid Mech.* (1991), *vol.* 227, *pp.* 293–308
*Printed in Great Britain*



# On cell formation in vortex streets

By BERND R. NOACK[1], FRANK OHLE[1]† AND HELMUT ECKELMANN[2]

[1] Max-Planck-Institut für Strömungsforschung, Bunsenstr. 10, D-3400 Göttingen, Germany

[2] Institut für Angewandte Mechanik und Strömungsphysik der Universität, Bunsenstr. 10, D-3400 Göttingen, Germany

(Received 30 April 1990)

A simple, phenomenological model is proposed for the formation of spanwise cells behind slender bodies of revolution in crosswise, uniform or non-uniform oncoming flow. The model yields estimates for the position of the cells, their frequencies, their amplitudes of oscillation along the span, and the local shedding angle. The qualitative features of the solutions of this theory agree well with experiments. A quantitative comparison with experiments for a slender cone is presented.

## 1. Introduction

Since Strouhal's (1878) discovery of 'aeolian tones', the vortex street behind bluff bodies has been a field of active research. The simplest example of this flow, the wake behind an infinitely long, circular cylinder in crosswise, uniform oncoming flow, is well understood. Experimental and numerical works suggest that the velocity field remains two-dimensional for Reynolds numbers less than about 160, being steady below and strictly periodic above 45. For Reynolds numbers greater than about 160, three-dimensional, irregular fluctuations are superimposed on the dominant periodic vortex shedding.

For a long time it was generally believed that the two-dimensional, laminar vortex street could be experimentally realized in the central region of a cylinder with a sufficiently large length-to-diameter ratio. Therefore, many observations, for instance the discontinuities in the Strouhal–Reynolds-number relationship (Tritton 1959; Berger 1964), were incorrectly attributed to different modes of two-dimensional vortex shedding. Gaster (1969, 1971) found similar discontinuities for a section of a cone and reasoned that the so-called Tritton jump is caused by a spanwise inhomogeneity in the flow field. König (1988), Williamson (1989), and König, Eisenlohr & Eckelmann (1990) could identify these discontinuities conclusively as an end effect, originating from the boundary layer at the wind tunnel walls. These end effects cannot be neglected, even if the aspect ratio is of the order of 100.

Thus, deviations from the ideal two-dimensional boundary conditions, for instance cylinder end plates, a non-uniform oncoming flow, or a spanwise-varying local diameter (e.g. cone), induce global changes along the cylinder. These spanwise inhomogeneities lead to the formation of cells, i.e. spanwise regions with constant shedding frequency. At the boundary between two cells, called *nodes*, this frequency changes discontinuously. This spanwise structure was first reported by Gaster (1971) for a cone and by Gerich (1979) and Gerich & Eckelmann (1982) near an end plate

† Present address: Beckman Institute, Center of Complex System Research, 405 North Mathews Avenue, Urbana, IL 61801, USA.

for a circular cylinder or a free-ended cylinder. Furthermore, the formation of cells also occurs when wind tunnel walls are used as side limitations.

In the present paper, a simple, phenomenological model is proposed for the near wake of a long body of revolution in non-uniform oncoming flow. This model yields many of the experimentally observed features, including the cell structure. Furthermore, the vortex formation behind the body can be predicted. Besides Gaster's (1969) model with a continuous chain of oscillators with a spanwise stiffness, the authors do not know of any previous successful attempt to explain these phenomena.

## 2. A model of cell formation

We consider the wake behind an axisymmetric body in crosswise, non-uniform, oncoming flow. For the following discussion a Cartesian coordinate system $x, y, z$ with the unit vectors $\hat{\boldsymbol{e}}_x, \hat{\boldsymbol{e}}_y, \hat{\boldsymbol{e}}_z$ is taken in which the $z$-axis coincides with the axis of symmetry of the body $B$ of length $L$. This body can thus be described by a local diameter $D(z)$:

$$B = \{(x, y, z): \quad x^2 + y^2 \leqslant \tfrac{1}{4}D^2(z), \quad 0 \leqslant z \leqslant L\}.$$

Furthermore, the unperturbed shear flow $\boldsymbol{u}_\infty$ is aligned with the $x$-axis,

$$\boldsymbol{u}_\infty = u_\infty(z)\,\hat{\boldsymbol{e}}_x,$$

depending only on the spanwise coordinate $z$. The local diameter $D(z)$ and the speed $u_\infty(z)$ are assumed to be slowly varying functions of $z$, so that the near wake in a neighbourhood of $z_0 \in (0, L)$, sufficiently far from the ends, can be expected to be similar to the flow behind a circular cylinder with constant diameter $D(z_0)$ in uniform flow $\boldsymbol{u}_\infty(z_0)\,\hat{\boldsymbol{e}}_x$. Furthermore, we require that the local Reynolds number $Re\,(z) = D(z)\,u_\infty(z)/\nu$, where $\nu$ is the kinematic viscosity, remains less than 160 along the body. Thus the near wake can be expected to be laminar.

Under these conditions, experimental observations for the slender cone in uniform flow (Gaster 1971) and for the circular cylinder in non-uniform flow due to end effects (Gerich 1979; Gerich & Eckelmann 1982) suggest the formation of cells, i.e. the presence of spanwise regions in which the shedding frequencies are constant. The present model is an attempt to gain some insight into this phenomenon.

As a first, crude approximation, we assume the near wake to be a simply connected region $W$, with sections $S(z)$ parallel to the $(x, y)$-plane, in which the flow field can be approximated by $\boldsymbol{u} = v(z)\,\hat{\boldsymbol{e}}_y$ (figure 1). Downstream convection may be neglected in the dead-water region behind the body. Spanwise velocity fluctuations will not be considered either, because of the 'quasi-two-dimensional' assumptions for $D(z)$ and $u_\infty(z)$. The $W$-region, the 'engine' of the vortex shedding, may be modelled by a discrete set of equidistant fluid layers of area $S_i := S(z_i)$ at $z_i = i\Delta z$ for the $i$th layer, in which the mass $\rho S_i\,\Delta z$ of the fluid with density $\rho$ is concentrated. (The fact that $S(z)$ is used simultaneously for a two-dimensional set of points and for its area should not lead to misunderstandings). Later, the discretization will be removed by effecting a limit $\Delta z \to 0$.

The near-wake idealization for the flow field permits only a vertical motion of these layers, the displacement from the equilibrium position at time $t$ and location $z_i$ being denoted by $q(z_i, t)$, or, more briefly, by $q_i$ (figure 1). If the local Reynolds number $Re\,(z_i)$ is in the so-called *regular* range between 45 and 160, a periodic vortex shedding is observed for the corresponding two-dimensional problem. Therefore, if no friction

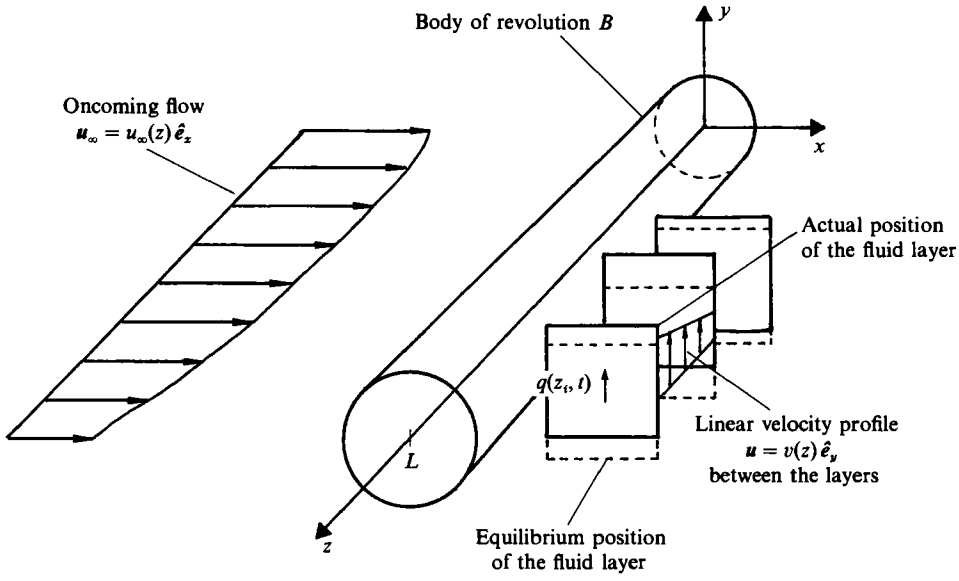


FIGURE 1. Sketch of the discrete fluid-layer model for the near wake behind a body of revolution in non-uniform oncoming flow.

between the layers is present, the displacements may be expected to have globally stable, periodic dynamics, like the van der Pol oscillator

$$\ddot{q}+\epsilon(q^2-1)\dot{q}+q=0. \tag{1}$$

Here, the dot denotes the differentiation with respect to time. The qualitative similarity of the dynamics of the two-dimensional vortex street and of this oscillator is often referred to as van der Pol analogy. In this analogy, the variable $q$ is usually not identified with a flow variable. In our model, (1) is assumed as the equation of motion for the displacement of the uncoupled fluid layer. In a similar manner, Skop & Griffin (1973, 1975) employed the van der Pol oscillator to describe the dynamics of the lift coefficient in a model for flow-induced vibrations of an elastically mounted cylinder. The question of whether other types of self-excited, amplitude-limited oscillators are more appropriate for our purposes will be considered in the next section.

Equation (1) has the approximate solution $q(t) = 2\sin t$ for small $\epsilon$ (Jordan & Smith 1988). Of course, the time and displacement have to be rescaled in the van der Pol equation in order to obtain an appropriate frequency and amplitude of the asymptotic solution. The natural frequencies $f_{0,i}$ of these oscillators are the shedding frequencies of the vortex street for the corresponding circular cylinder. For the regular range this shedding frequency $f$ is well approximated by Roshko's (1954) empirical formula

$$F = \frac{D^2}{\nu} f = 0.212\,Re - 4.5.$$

For Reynolds numbers less than 45 the flow is steady. In this case, $F$ may be set equal to zero. Thus, the frequency of the $i$th oscillator is given by

$$f_{0,i} = \begin{cases} \dfrac{\nu}{D^2(z_i)} F(Re\,(z_i)) & \text{for} \quad 45 \leqslant Re\,(z_i) \leqslant 160; \\ 0 & \text{for} \quad Re\,(z_i) < 45. \end{cases} \tag{2}$$

An appropriate choice for the amplitude $A_{0,i}$ of an uncoupled oscillator is

$$A_{0,i} = kD(z_i). \tag{3}$$

This implies that the amplitude of the velocity fluctuations increases in proportion to the local lengthscale, the diameter $D(z)$. Rescaling the dependent and independent variables of the van der Pol oscillator, (1), to get the approximate asymptotic solution $q_i = A_{0,i} \sin \Omega_{0,i} t$ with $\Omega_{0,i} = 2\pi f_{0,i}$ yields after multiplication with the mass of the fluid layer

$$\rho S_i \Delta z \left[ \ddot{q}_i + \epsilon \Omega_{0,i} \left( \frac{q_i^2}{\frac{1}{4} A_{0,i}^2} - 1 \right) \dot{q} + \Omega_{0,i}^2 q_i \right] = 0. \tag{4}$$

The first term may be interpreted as the inertia, i.e. mass times acceleration, the last one as a Hooke's restoring force, and the nonlinear term as an amplitude-limited excitation force.

In order to introduce a viscous coupling between these oscillators, we assume that there is a weightless Newtonian fluid with the dynamic viscosity $\mu$ between these layers. For small $\Delta z$ the one-dimensional velocity profile $v(z)$ in the $y$-direction of the fluid in the $W$-region may be considered as linear between $z_i$ and $z_{i+1}$, satisfying $v(z_i) = \dot{q}_i$ for all $i$, i.e. adhering to the oscillators. Then the force $f_{i\pm1\to i}$ of the $(i\pm1)$th layer on the $i$th one can easily be derived from the Navier–Stokes equation, if end effects at the boundary of $W$ are neglected. The result is

$$f_{i\pm1\to i} = \mu S_i \left( \frac{\dot{q}_{i\pm1} - \dot{q}_i}{\Delta z} \right),$$

as for the forces between two moving parallel plates with a Newtonian fluid between them. The forces of the right and left neighbours on the $i$th oscillator have to be added to the right-hand side of (4). Thus, we get an equation of motion for a system of coupled oscillators:

$$\rho S_i \Delta z \left[ \ddot{q}_i + \epsilon \Omega_{0,i} \left( \frac{q_i^2}{\frac{1}{4} A_{0,i}^2} - 1 \right) \dot{q}_i + \Omega_{0,i}^2 q_i \right] = \mu S_i \left( \frac{\dot{q}_{i+1} - 2\dot{q}_i + \dot{q}_{i-1}}{\Delta z} \right).$$

Dividing this equation by $\rho S_i \Delta z$ and applying

$$\lim_{\Delta z \to 0} \frac{f(z+\Delta z) - 2f(z) + f(z-\Delta z)}{\Delta z^2} = \frac{\mathrm{d}^2 f}{\mathrm{d}z^2},$$

we obtain with (2) and (3) the corresponding continuous version

$$\frac{\partial^2 q}{\partial t^2} + \epsilon \Omega_0 \left( \frac{q^2}{\frac{1}{4} A_0^2} - 1 \right) \frac{\partial q}{\partial t} + \Omega_0^2 q = \nu \frac{\partial^3 q}{\partial z^2 \, \partial t}, \tag{5a}$$

with the frequency distribution

$$\omega_0(z) = \begin{cases} 2\pi \dfrac{\nu}{D^2(z)} F(Re\,(z)) & \text{for} \quad 45 \leqslant Re\,(z) \leqslant 160; \\ 0 & \text{for} \quad Re\,(z) < 45; \end{cases} \tag{5b}$$

and the amplitude distribution

$$A_0(z) = kD(z). \tag{5c}$$

This is a parabolic partial differential equation for $q(z,t)$ with diffusion of the velocity $v = \partial q/\partial t$ in the spanwise direction and self-excited, amplitude-limited periodic dynamics for each $z$ if $Re\,(z) > 45$. If $Re\,(z) < 45$ for all $z$, the frequency vanishes, $\Omega(z) \equiv 0$, and (5$a$) reduces to a simple diffusion equation in the velocity

component in the $y$-direction, $v = \partial q/\partial t$. This diffusion equation can, of course, be derived directly from the Navier–Stokes equation for one-dimensional, plane-parallel flow without an exterior pressure gradient.

It may be interesting to note that Gaster's (1969) spanwise stiffness term $\alpha(\partial^2 q/\partial z^2)$ can similarly be derived by assuming elastic (non-dissipative) forces

$$f_{i\pm1\to i} = \alpha\Delta z(q(z_{i\pm1}, t) - q(z_i, t))$$

between the layers. These forces correspond to a coupling between consecutive oscillators with springs of restoring constant $\alpha\Delta z$.

Equation (5) defines the equation of motion for a given experimental set-up. The undetermined constant $k$ in (5$c$) can be removed by a normalization of the independent and dependent variables with the natural amplitude $A_{\text{ref}} := A_0(z_{\text{ref}}) = kD_{\text{ref}}$ with $D_{\text{ref}} := D(z_{\text{ref}})$ and the natural frequency $f_{\text{ref}} = 1/T_{\text{ref}} := f_0(z_{\text{ref}})$ at an appropriate reference point $z_{\text{ref}}$. Introducing $\zeta := z/L$, $\tau := t/T_{\text{ref}}$, and $\eta(\zeta, \tau) := q(\zeta L, \tau T_{\text{ref}})/A_{\text{ref}}$, we get the non-dimensional form of (5)

$$\frac{\partial^2\eta}{\partial\tau^2} + \epsilon\omega_0\left(\frac{\eta^2}{\frac{1}{4}\alpha_0^2} - 1\right)\frac{\partial\eta}{\partial\tau} + \omega_0^2\eta = \kappa\frac{\partial^3\eta}{\partial\zeta^2\,\partial\tau}, \tag{6$a$}$$

where

$$\omega_0(\zeta) = 2\pi\frac{f_0(\zeta L)}{f_{\text{ref}}}, \tag{6$b$}$$

$$\alpha_0(\zeta) = \frac{A_0(\zeta L)}{A_{\text{ref}}} = \frac{D(\zeta L)}{D_{\text{ref}}}, \tag{6$c$}$$

and $\kappa = \nu T_{\text{ref}}/L^2$ represents the coupling coefficient.

If the body is of finite length, say $L$, the boundary conditions have to be specified. When the axisymmetric body is bounded by an end plate, which is parallel to the $(x, y)$-plane, say at $z = 0$, the layer at this end cannot move, because of the no-slip condition. Hence, the Dirichlet boundary condition

$$q(0, t) \equiv 0 \quad \text{(fixed end)} \tag{7$a$}$$

satisfies the no-slip condition for the velocity $v(0, t) = \partial q(0, t)/\partial t = 0$ for this 'fixed end'. For a free-ended body, the stress-free Neumann condition $\partial v(0, t)/\partial z = \partial^2 q(0, t)/\partial t\,\partial z = 0$ seems to be appropriate. If $q(0, 0) = 0$, integration over $t$ yields

$$\frac{\partial q(0, t)}{\partial z} = 0 \quad \text{(free end)}. \tag{7$b$}$$

The simplifications of this model are, of course, crude. For instance, we assume the existence of a region where the flow can be approximated by $\boldsymbol{u}(\boldsymbol{x}, t) = v(z, t)\,\hat{\boldsymbol{e}}_y$ and, furthermore, that the viscous coupling takes place in this region. The influence of the surrounding fluid has not been taken into account. Hence, an exact quantitative agreement between the model and the experiment cannot be expected. For example, the coupling coefficient for which the kinematic viscosity has been taken may be incorrect by a factor of the order of unity. Nevertheless, the idealizations do not seem to be in conflict with the qualitative coupling mechanism. Therefore, a qualitative agreement with experimental results can be expected.

## 3. Qualitative features of the model

In this section, we analyse the numerical solutions of the model and compare the results qualitatively with experiments. The equation of motion of this model has been solved for a wide variety of experimental set-ups, including different bodies of

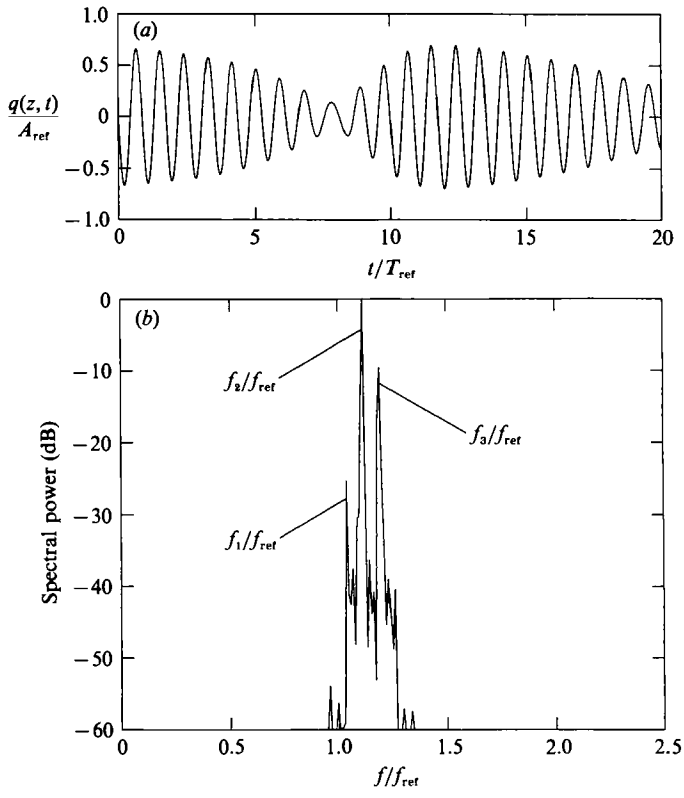


FIGURE 2. (*a*) The non-dimensional displacement $q(z,t)$ at $z/L = 0.215$ as a function of the normalized time $t$ and (*b*) its power spectrum from the numerical solution of (5) and (7*b*) for a cone in uniform flow. The local Reynolds numbers varies from 59.7 at the diameter $D_2 = 1$ mm ($z = L = 20$ mm) to 179.2 at the diameter $D_1 = 3$ mm ($z = 0$). Displacement, time, and frequency are non-dimensionalized with the natural amplitude, period, and frequency at $D_1$, respectively. The nonlinearity parameter is $\epsilon = 0.2$. The nearly periodic time function $t \mapsto q(z,t)$ has the dominating frequency $f_2$ of the second cell, the amplitude varies with the beat frequency $f_3 - f_2$. The corresponding power spectrum shows discrete major peaks at the dominating frequencies of the first, second, and third cell, $f_1$, $f_2$, and $f_3$.

revolution in uniform flow, a cylinder with end plates (Noack 1989), and a cylinder in spanwise shear flow. It turns out that these solutions have universal properties which are independent of the particular set-up and which can also be observed in experiments. We will discuss these features for a simple example, a section of a cone of length $L = 20$ mm with the local diameters $D_1 = D(0) = 3$ mm and $D_2 = D(L) = 1$ mm at its ends in uniform flow with velocity $u_\infty = 0.89$ m/s. Taking the kinematic viscosity for air at a temperature of 20° C, $\nu = 14.9 \times 10^{-6}$ m$^2$/s, the local Reynolds numbers remain near the regular range, the minimal and maximal values being $Re(0) \approx 59.7$ and $Re(L) \approx 179.2$.

From the given data, the natural frequency and amplitude distribution can be derived from (5*b*, *c*). (Without loss of generality the constant in (5*c*) may be set equal to unity, since we consider only non-dimensionalized displacements $q$.) The frequency doubles from $z = 0$ to $z = L$, whereas the amplitude decreases by a factor of $D_2/D_1 = \frac{1}{3}$. Thus, the adjustable functions in the equation of motion (5*a*) are determined. As boundary conditions for $z = 0$ and $z = L$, equation (7*b*) for a free end is employed. The initial conditions for $q(z,0)$ and $\partial q(z,0)/\partial t$ at $t = 0$ are not crucial,

since the solution displays an asymptotic behaviour, which is independent of the initial conditions after a sufficiently long time. Although the transient behaviour is interesting, the discussion will be restricted to the asymptotic solution, which is better understood experimentally.

The choice of the nonlinearity parameter $\epsilon$, which is a measure of the 'strength' of the oscillator in comparison with the coupling forces, has a strong influence on the asymptotic solution. Generally, the actual amplitude

$$A(z) \overset{\text{def}}{=} \lim_{T\to\infty} \left(\frac{2}{T}\int_0^T q^2(z,t)\,\mathrm{d}t\right)^{\frac{1}{2}}$$

increases with $\epsilon$, but always remains smaller than the natural amplitude $A_0(z)$ of the uncoupled oscillator. The inequality $A(z) \leqslant A_0(z)$ for $z \in (0, L)$ has been proved analytically using perturbation methods (Noack 1989). If no friction is present ($\nu = 0$), we get $A(z) = A_0(z)$. This can easily be verified by substituting the approximate solution of the uncoupled oscillator (4) in the definition of $A(z)$. Furthermore, the dominating frequency $f(z)$, defined by the maximum in the power spectrum of the time function $t \mapsto q(z,t)$ for fixed $z$, tends to be closer to the natural frequency $f_0(z)$ with increasing $\epsilon$, i.e.

$$\max_{z\in(0,\,L)} |f(z) - f_0(z)|$$

decreases, whereas the number of cells increases. Without a coupling ($\nu = 0$), the dominating and natural frequencies are equal, i.e. $f(z) = f_0(z)$.

In the present example we set $\epsilon = 0.2$. This value is large enough to ensure that $A(z)$ is not much smaller than $A_0(z)$, so that the 'quasi-two-dimensional' assumption for the spanwise inhomogeneity is extended to the solution of this model. On the other hand, it is small enough so that the approximations for $A_0(z)$ and $f_0(z)$ of the solution of the van der Pol oscillator for small $\epsilon$ remain accurate to the order of 0.1 %.

We start the discussion of the numerical solution of the model for a cone (see above) with graphs of the time functions $q_z(t) := q(z,t)$ for fixed $z$ and their power spectra (figures 2 and 3). The displacement $q$, the time $t$, and the frequency $f$ are non-dimensionalized with the reference values at $z = 0$, i.e. $A_{\text{ref}} = A_0(0)$, $T_{\text{ref}} = 1/f_0(0)$ and $f_{\text{ref}} = f_0(0)$, respectively. Figure 2(*a*) shows an oscillation with a periodically changing amplitude. This behaviour may be called 'nonlinear beat'. The corresponding power spectrum seems to be discrete, with major peaks at $f_1, f_2$ and $f_3$. The highest peak at $f_2$ determines the period of oscillation; the difference between the positions of the two highest maxima, $f_3 - f_2$, determines the period of the nonlinear beat. For increasing $z$, i.e. increasing natural frequency $f_0(z)$ in this case, the maximum at $f_3$ increases in comparison with the one at $f_2$. Finally, the power spectrum has two global maxima (figure 3*b*). At this position, called a *node*, the time function (figure 3*a*) is completely modulated and has phase jumps. Increasing $z$ further, the dominating frequency is $f_3$, until we arrive at another node, and so on. The same phenomena, including discrete spectra, nonlinear beat, and phase jumps at the nodes, have been reported for experimental velocity fluctuations behind a circular cylinder with two end plates (Gerich 1979; Gerich & Eckelmann 1982; Williamson 1989; König *et al.* 1990). These phenomena seem to be universal for vortex shedding behind bluff bodies with a spanwise inhomogeneity of the body or the oncoming flow (Gaster 1971; A. Papangelou 1990, private communication).

Figure 4(*a*) displays the dominating and natural frequency and figure 4(*b*) the amplitude distribution. Furthermore, the phase shifts within the cells are visualized

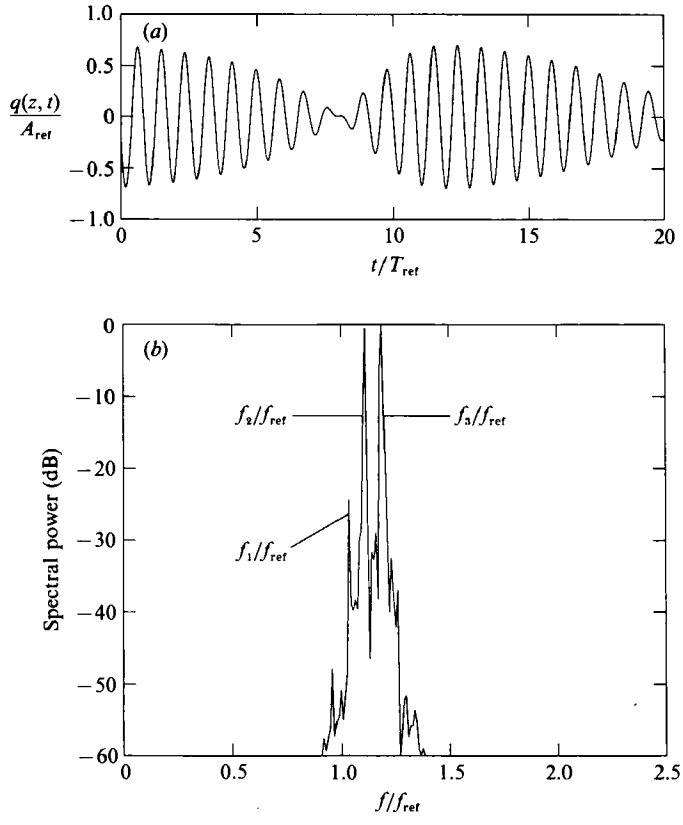


FIGURE 3. Same as figure 2, but for $z/L = 0.235$ at a node.

in figure 4(*c*). Figure 4(*a*) indicates the presence of a partition $0 = z_0 < z_1 < \ldots < z_N = L$, such that $f(z) = f_i$ is constant in a cell $(z_{i-1}, z_i)$ and has a discontinuity of the first kind (finite jump) at the nodes $z_i$. The amplitude (figure 4*b*), tends to decrease at the nodes owing to the occasional confinement of the time function $q_z(t)$. Figure 4(*c*) displays the extrema of $(z,t) \mapsto q(z, t_0 - t)$ with respect to $t$ for all values of $z$, i.e. the points with $\partial q/\partial t = 0$. Here, $t_0$ denotes a reference time, so that the bottom line $t - t_0 = 0$ of the graph represents 'the present' ($t = 10$) and the top line $t - t_0 = 10$ 'the past' ($t = 0$). The solid curves represent the maxima ($\partial^2 q/\partial t^2 < 0$), the dotted ones the minima ($\partial^2 q/\partial t^2 > 0$). Within a cell these points form a set of nearly parallel curves. the inclinations of these curves indicate a phase shift in the cell; the oscillators with the higher natural frequencies tend to 'move ahead'. At the nodes $z = z_i$, where the dominating frequency $f(z)$ or, equivalently, the dominating period $T(z) = 1/f(z)$ has a discontinuity, the curves usually continue into the other cell. Occasionally, however, the number of extrema are reduced from three to one at the node, when three curves coalesce into one. Sometimes, a maximum and minimum cancel each other, leaving a point of inflexion at the node. In any case, the number of extrema can only change by two (or multiples thereof), since no maximum of $q_z(t)$ can be created without a minimum, and vice versa.

The graph in figure 4(*c*) resembles the vortex patterns in flow visualizations. This coincidence is not accidental. Suppose that the $z$-axis, the axis of symmetry of the body, coincides with $t = t_0$ at the bottom of the frame, and the $x$-axis, the direction of the oncoming flow, is parallel to the ordinate of this plot. If the fluid in the near

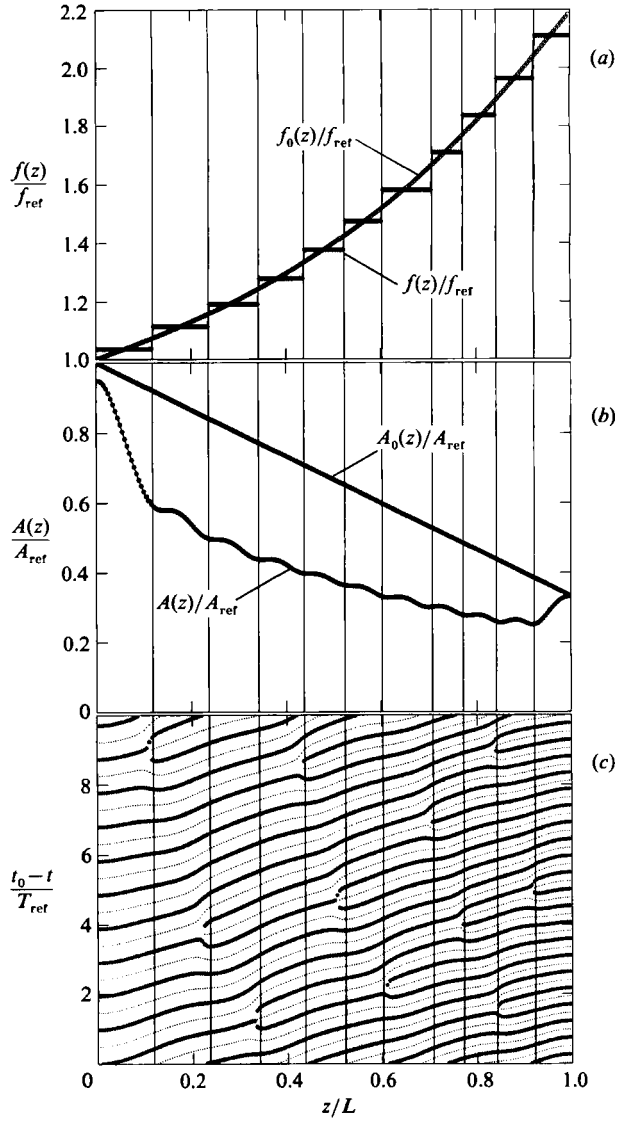


FIGURE 4. Summary of the main features of the numerical solution for parameters given in figure 2. The variables are normalized as in figure 2. (*a*) Comparison between the dominating frequency $f(z)$ of the cell formation and the natural frequency $f_0(z)$ from Roshko's (1954) formula as a function of the spanwise coordinate. (*b*) The actual and natural amplitudes, $A(z)$ and $A_0(z)$. (*c*) The maxima (solid lines) and minima (dotted lines) of the time function $t \mapsto q(z, t_0 - t)$ along the span of the cone. These curves can be interpreted as a vortex formation (see text).

wake (in the neighbourhood of some $z_0$) moves up (out of the paper or, in terms of the model, $\partial q/\partial t > 0$), a vortex originates at the lower side of the cone; if it moves in the negative $y$-direction ($\partial q/\partial t < 0$) an oppositely oriented vortex emerges at the upper side of the body. Assuming that the vorticity is convected downstream with constant speed of propagation $c$, the minima of $q(z, x/c - t)$ with respect to the second coordinate correspond to clockwise-oriented vortices at distance $x$ from the body at time $t$, whereas the maxima represent vortices of positively oriented circulation. The dimension of the body is neglected in this reasoning. Thus, the non-dimensionalized

ordinate $(t_0-t)/T_{\mathrm{ref}}$ is – modulo a factor $cT_{\mathrm{ref}}$ – the distance from the body, and the curves can be interpreted as the projection of the vortex formation on the $(x,z)$-plane. In this $(x,z)$-plane the local shedding angle is the tangent of slope of the curves. Assuming the propagation speed of the vortices to be slightly lower than the oncoming velocity, say $c = 0.8u_\infty$, a typical angle for the present example is about 60°. Generally, this angle of the numerical solution increases with increasing strength of the oscillator, i.e. $\epsilon$, the other parameters being fixed. The angle decreases with decreasing length of the cone, i.e. increasing non-dimensionalized coupling strength. The occasional coalescence of these curves can be regarded as a vortex splitting (Eisenlohr & Eckelmann 1989). This phenomenon has also been called 'vortex dislocation' (Williamson 1989) – in analogy to dislocations in solid state physics. From the inclination of these lines the shedding angle can be computed.

In order to discuss the influence of the choice of the oscillator on the solution of the model, we consider a van der Pol oscillator with a strongly nonlinear restoring force,

$$\frac{\mathrm{d}^2q}{\mathrm{d}t^2}+\epsilon(q^2-\tfrac{1}{4})\frac{\mathrm{d}q}{\mathrm{d}t}+\tfrac{1}{2}q+\tfrac{2}{3}q^3 = 0. \tag{8}$$

An approximate asymptotic solution of this equation is $q = \sin t$, as can easily be verified with the harmonic balance method by neglecting higher harmonics. Rescaling the dependent and independent variables as in (4) and adding the coupling term yields a partial differential equation which corresponds to (5*a*). The numerical solution of this equation for the experimental set-up, described in figures 2–4, is illustrated in figure 5. We get 9 cells as compared with 11 in figure 4. The dominating frequency is always smaller than the natural frequency (figure 5*a*), since the cubic stiffness terms in (8) gives rise to lower frequencies for lower amplitudes and the amplitudes (figure 5*b*) are reduced by the coupling. Near the vortex splitting (figure 5*c*), where the amplitude of oscillation is very small and hence the frequency significantly reduced, the 'shedding angle' may change its sign, since the oscillators in the centre of cell with the higher local frequency want to move ahead. A variety of other self-excited, amplitude-limited oscillators have been tested, but the qualitative features are not affected by this choice. The example given, with a pronounced amplitude-frequency relationship due to a nonlinear potential, is even a bit extreme.

Having discussed the numerical solution of (5) for one set of physical parameters, the oncoming velocity $u_\infty$, the diameters $D_1$ and $D_2$ at the ends of the cone and its length $L$, and one free parameter of the model $\epsilon$, the question arises as to what extent the solution is affected by a change of these parameters. Numerous numerical experiments seem to indicate that no qualitatively new phenomena occur. In all cases considered, we get a formation of cells with the properties described above. Nevertheless, the number of cells depends sensitively on these parameters, especially on $\epsilon$ and $L$. Since the influence of $\epsilon$ on the asymptotic solution has already been outlined, we restrict the discussion to the influence of $L$, keeping the other parameter fixed, i.e. $\epsilon = 0.2$, $D_1 = 3$ mm, $D_2 = 1$ mm and $u_\infty = 0.89$ m/s. In other words, we 'stretch' the cone uniformly along its axis of revolution. In the non-dimensional equation of motion (6), this stretching changes only the coupling coefficient $\kappa = \nu/f_{\mathrm{ref}}L^2$, leaving the natural frequencies and amplitudes in terms of $\zeta = z/L$ unaltered. We expect the number of cells to increase with decreasing coupling coefficient, i.e. increasing $L$. This expectation is confirmed by figure 6(*a*) in which the number of cells $N(L)$ is shown in terms of $L$. $N(L)$ is a monotonically increasing staircase function,

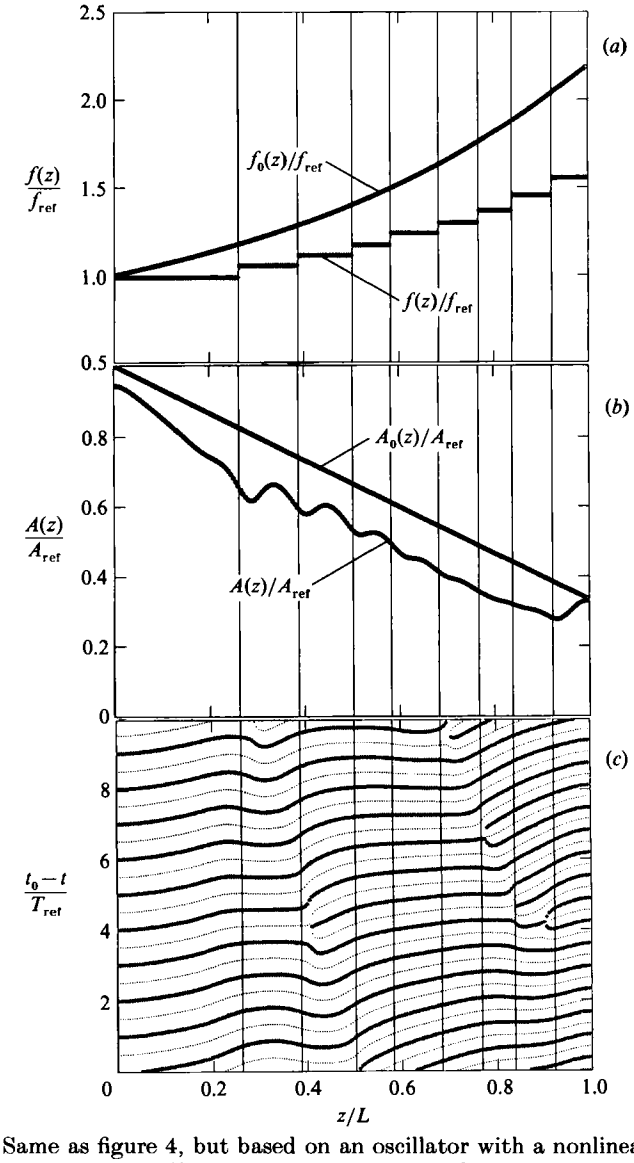


FIGURE 5. Same as figure 4, but based on an oscillator with a nonlinear restoring force. Equation (8) is used instead of (1).

with discontinuities at a discrete set $\{L_k\}$ of lengths. Usually, the number of cells increases one by one, so cells do not seem to originate simultaneously. Each 'new' cell gives rise to a new frequency in the spectrum $\{f_i(L)\}_{i=1}^{N(L)}$. The 'old' frequencies change continuously without a kink at the critical values $L_k$ (see figure 6*b*). The 'new' cells in the partition $0 = x_0(L) < x_1(L) < \ldots < x_{N(L)}(L) = L$ (figure 6*c*) seem to be created at the boundary of two 'old' ones; the extent of the newcomer increases continuously from 0 at $L_k$. The other boundaries $z_i$ show no jumps or kinks. Thus, the birth of a cell is a local event which does not lead to global changes along the span width. It is worthwhile to note that the manner in which cells are created or destroyed does not seem to depend on the choice of the variable parameters or on the set-up considered. A continuous change of the oncoming flow, for instance, appears to yield

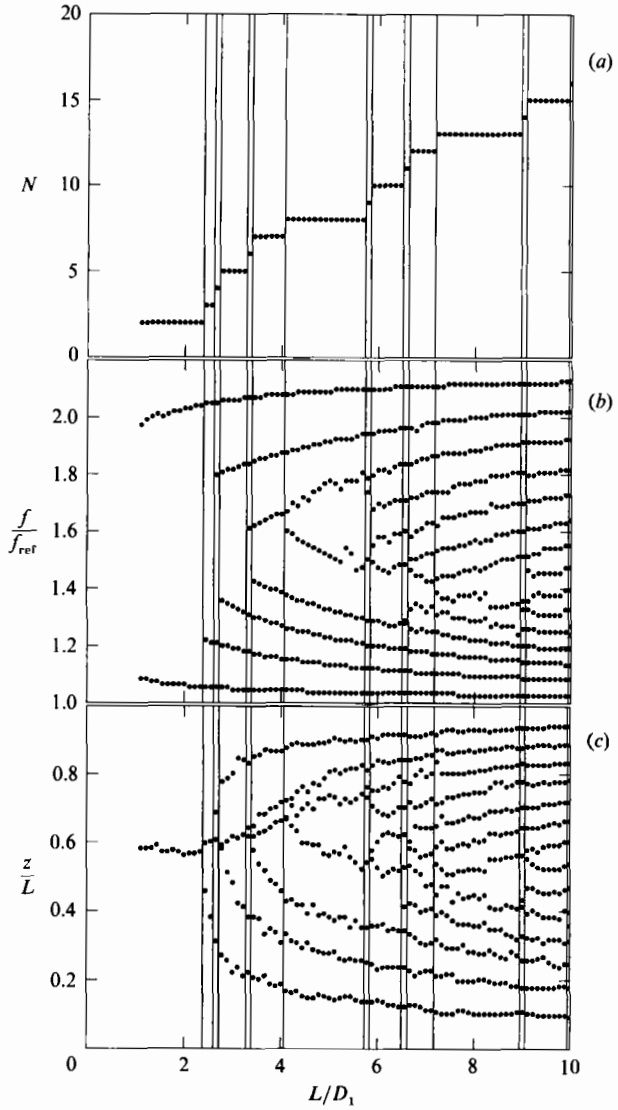


FIGURE 6. Influence of the non-dimensional length $L$ on the cell formation of a cone in uniform flow (see figure 2 for details). (*a*) The number of cells $N(L/D_1)$ increases monotonically with the length of the cone $L$, the other parameters, i.e. $D_1$, $D_2$, $u_\infty$, $\nu$ and $\epsilon$, being fixed. The corresponding dominating frequencies $\{f_i(L/D_1)\}_{i=1}^{N(L/D_1)}$, (*b*), and nodes $\{z_i(L/D_1)\}_{i=1}^{N(L/D_1)-1}$, (*c*), yield continuous curves.

similar bifurcations. These results are in qualitative agreement with experimental observations for a cylinder with two end plates, where the Reynolds number is chosen as the variable parameter (Williamson 1989; König *et al.* 1990) and for a cone in variable oncoming velocity (A. Papangelou 1990, private communication).

## 4. Comparison between model and experiment

The solution of the partial differential equation (5) contains many qualitative features found in experimental velocity fluctuations behind bluff bodies. In the case of a body of revolution in a crosswise oncoming shear flow, the model also yields

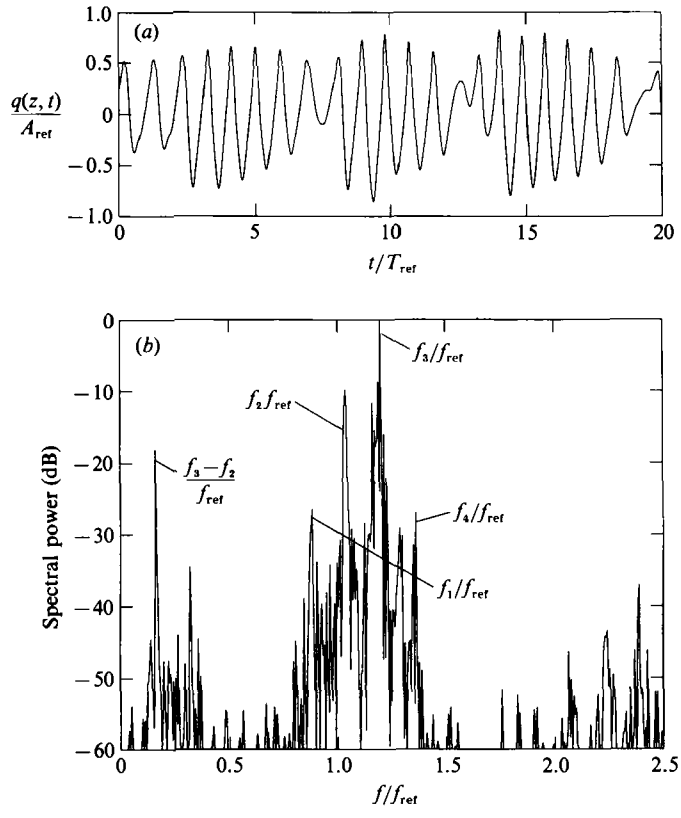


FIGURE 7. Same as figure 2, but experimentally obtained. The hot-wire probe was located 70 mm from the base ($z/L = 0.389$), three local diameters downstream, and two diameters above the axis of symmetry of the cone. The reference amplitude $A_{ref}$ is chosen to be the maximal velocity deviation from its average.

quantitative predictions about the number of cells, their frequencies and positions, and the local shedding angle of the vortex lines. The question arises as to how well these results agree with experiments. In order to check the validity of our model, we investigated the near wake behind a cone in a wind tunnel. The open-circuit-type wind tunnel has a circular nozzle of diameter 180 mm. The tunnel is described in Detemple-Laake & Eckelmann (1989). Further technical details may also be found in Ohle (1989). The end diameters of the cone of length $L = 180$ mm are $D_1 = 3$ mm and $D_2 = 1$ mm, respectively. This cone is placed directly behind the nozzle exit of the wind tunnel so that the whole span is immersed in the flow. The local Reynolds number varies linearly from 59.7 to 179.2 at the base.

All velocity fluctuations in the $x$-direction are measured two local diameters above and three behind the body, i.e. at $(x, y, z) = (3D(z), 2D(z), z)$. They show a nonlinear beat (figure 7*a*), which was also obtained in the numerical solution (figure 2*a*). In contrast to the model, the experimental oscillations are not symmetrical with respect to the average (here 0), since the hot-wire probe is located in one 'side' of the wake and not in the middle. The corresponding power spectrum (figure 7*b*) is nearly discrete, as in figures 2(*b*) and 3(*b*), having a global maximum at $f_3$, the shedding frequency of the considered, third cell, and smaller peaks at the frequencies of the neighbouring cells, $f_2$ and $f_4$. Furthermore, peaks at integral linear combinations of these frequencies can be found. The most noticeable combination is the beat $f_3 - f_2$,

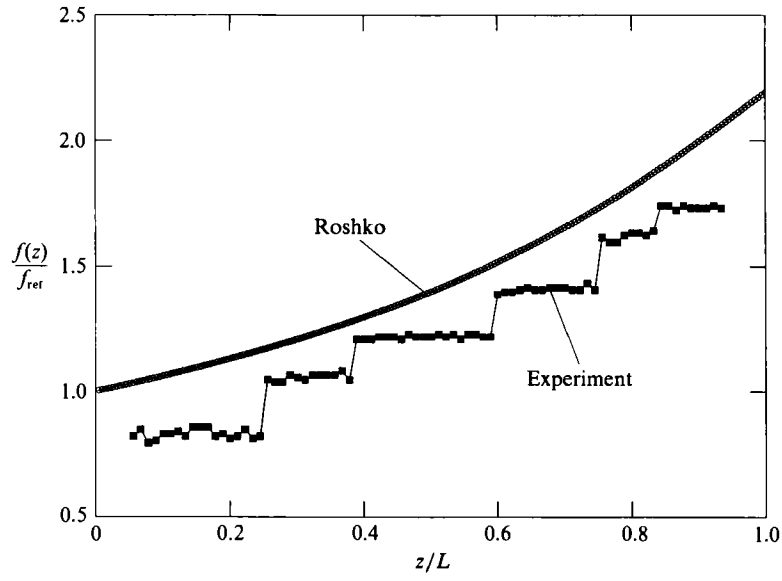


FIGURE 8. Experimentally determines dominating frequency along the span in comparison with the natural frequency, given by Roshko's (1954) formula for the regular range. Further details are given in figure 7.

which is characteristic for the asymmetry of the oscillation. The power spectrum contains many other peaks of low intensity, since the positions of the cell boundaries fluctuate owing to small, non-steady perturbations of the oncoming flow, which cannot be completely avoided.

The dominating frequency distribution along the body (figure 8) indicates the formation of six cells. The size of these cells seems to decrease with the local diameter, i.e. increasing $z$, whereas both end cells are comparatively large. These tendencies can also be found in the model (figure 4). The experimentally observed frequencies are always lower than the values obtained with Roshko's formula, in agreement with Gaster's (1969) results, but in contrast to the model. This discrepancy may be explained by considering the amplitude–frequency characteristics of the van der Pol oscillator and the two-dimensional wake behind a cylinder. The frequency of the latter decreases with decreasing amplitude, as can be shown by averaging methods from reconstructed differential equations of experimental time series of the flow behind a cylinder (Ohle 1989). For the van der Pol equation, however, the frequency increases with decreasing amplitude. Thus the experimental frequency of the reduced amplitude (due to the coupling) should be lower than the one from the continuous chain of van der Pol oscillators. Another explanation for the experimentally obtained difference between the natural and actual frequencies can be obtained from the observation of slanted vortex shedding within a cell. For a circular cylinder the ratio between the non-dimensional frequency $F$ for slanted vortex shedding with a shedding angle $\phi$ and the frequency $F_0$ for two-dimensional flow at the same Reynolds number decreases with $\phi$ according to Williamson's (1988) formula

$$F(Re) = F_0(Re)\cos\phi.$$

Hence, for our quasi-two-dimensional boundary condition, it is natural also to expect a lower actual shedding frequency than the one obtained from Roshko's (1954) formula due to the slanted shedding.

Another discrepancy between *ars et usus* is the number of cells. In the experiment we get six cells, whereas the corresponding partial differential equation (with free ends) yields more than a hundred for $\epsilon = 0.2$. Approximately six cells in the model are found for a higher taper, $L = 10$ mm (figure 6). This difference can be reduced by introducing an appropriate factor $p > 1$ in the coupling strength so that the right-hand side of (5*a*) reads $p\nu\partial^3 q/\partial t\,\partial z^2$. Realizing that the number of cells $N$ is only a function of the non-dimensionalized coupling strength in (6), $\kappa = p\nu/f_{\text{ref}}L^2$, the new parameter is easily seen to be $p = (180/10)^2 = 324$. With this correction, the theoretically predicted shedding angle of the model also lies in the experimentally observed range of 20°–25°. Nevertheless, this factor is surprisingly high and indicates that other physical processes contribute to the coupling strength. A possible explanation is that the microscopic momentum exchange, the molecular friction, is much smaller than the macroscopic momentum exchange because of (not necessarily large) spanwise velocity components. The latter is also a diffusion process in the velocity, so that the form of the spanwise coupling remains the same, except that another diffusion coefficient must be used. Another reason for this large correction factor may be the choice of the strength of the oscillator $\epsilon$. The larger the value of $\epsilon$, the more cells are formed. For $\epsilon = 0.1$, for instance, we obtain a smaller correction factor $p \approx 80$. Thus, if the chosen value of $\epsilon$ is too large, the correction factor will be too large also. In any case, the agreement between theory and experiment is fairly close, if the same factor is used for cones of other dimensions (H. Eisenlohr 1990, private communication). It may be that this correction is applicable with satisfactory results to a wide variety of bodies of revolution. Further experimental research and theoretical explanations for the spanwise coupling are in progress.

## 5. Conclusion

The proposed model yields all qualitative features found in experiments, including the formation of cells, a reduced amplitude of oscillation due to the coupling, discrete power spectra, nonlinear beat near the cell boundaries, slanted vortex shedding within a cell, and the presence of vortex splitting. Furthermore, the way in which cells are created or destroyed with a variable control parameter is in qualitative agreement with experiments. In order to reach quantitative agreement, at least with respect to the number of cells, the coupling coefficient factor $p$ may have to be varied. This factor is a measure of the actual coupling coefficient as compared to a simplified viscous coupling. Thus, from the fit of $p$ for a given experimental data we get additional physical information. Further improvements of the model are needed to obtain accurate estimates, for instance, for the shedding frequencies, but it is adequate to give us a rough idea about the structure of the laminar near wake behind a slender body with a slowly varying spanwise inhomogeneity.

We are grateful to Erika Roesch for providing us with her data acquisition utilities. We acknowledge valuable discussions with Professor Obermeier, Professor Fiszdon, Holger Eisenlohr and Ares Papangelou. The numerical computations have been performed with computers of the Gesellschaft für Wissenschaftliche Datenverarbeitung, Göttingen and of the Max-Planck-Institut für Strömungsforschung, Göttingen.

## REFERENCES


BERGER, E. 1964 Die Bestimmung der hydrodynamischen Grössen einer Kármánschen Wirbelstraße aus Hitzdrahtmessungen bei kleinen Reynoldsschen Zahlen. *Z. Flugwiss.* **12**, 41–59.

DETEMPLE-LAAKE, E. & ECKELMANN, H. 1989 Phenomenology of Kármán vortex streets in oscillatory flow. *Expts Fluids* **7**, 217–227.

EISENLOHR, H. & ECKELMANN, H. 1989 Vortex splitting and its consequences in the vortex street wake of cylinders at low Reynolds numbers. *Phys. Fluids* A **1**, 189–192.

GASTER, M. 1969 Vortex shedding from slender cones at low Reynolds numbers. *J. Fluid Mech.* **38**, 565–576.

GASTER, M. 1971 Vortex shedding from circular cylinders at low Reynolds numbers. *J. Fluid Mech.* **46**, 749–756.

GERICH, D. 1979 Einfluß von Endscheiben und freien Enden auf den Nachlauf von angeströmten Zylindern. Diplomarbeit, Institut für Angwandte Mechanik und Strömungsphysik der Georg-August-Universität, Göttingen.

GERICH, D. & ECKELMANN, H. 1982 Influence of end plates and free ends on the shedding frequency of circular cylinders. *J. Fluid Mech.* **122**, 109–121.

JORDAN, D. W. & SMITH, P. 1988 *Nonlinear Ordinary Differential Equations*, chap. 4. Clarendon.

KÖNIG, M. 1988 Diskontinuitäten im Nachlauf von Kreiszylindern bei kleinen Reynoldszahlen. Diplomarbeit, Institut für Angwandte Mechanik und Strömungsphysik der Georg-August-Universität, Göttingen.

KÖNIG, M., EISENLOHR, H. & ECKELMANN, H. 1990 The fine structure in the Strouhal–Reynolds number relationship of the laminar wake of a circular cylinder. *Phys. Fluids* A **2**, 1607–1614.

NOACK, B. R. 1989 Untersuchung chaotischer Phänomene in der Nachlaufströmung eines Kreiszylinders. Diplomarbeit, Institut für Angwandte Mechanik und Strömungsphysik der Georg-August-Universität, Göttingen.

OHLE, F. 1989 Beschreibung transienter Zustände der Kármánschen Wirbelstraße und Anregung der Wirbelstraße durch Schall. Diplomarbeit, Institut für Angwandte Mechanik und Strömungsphysik der Georg-August-Universität, Göttingen.

ROSHKO, A. 1954 On the development of turbulent wakes from vortex streets. *Natl Advisory Comm. Aeronaut.* TN 1191.

SKOP, R. A. & GRIFFIN, O. M. 1973 A model for the vortex-excited resonant response of bluff cylinders. *J. Sound Vib.* **27**, 225–233.

SKOP, R. A. & GRIFFIN, O. M. 1975 On a theory for the vortex-excited oscillations of flexible cylindrical structures. *J. Sound Vib.* **27**, 263–274.

STROUHAL, V. 1878 Über eine besondere Art der Tonerzeugung. *Ann. Phys. Chem.* (Neue Folge) **5**, 215–251.

TRITTON, D. J. 1959 Experiments on the flow past a circular cylinder at low Reynolds numbers. *J. Fluid Mech.* **6**, 547–567.

WILLIAMSON, C. H. K. 1988 Defining a universal and continuous Strouhal–Reynolds number relationship for the laminar vortex shedding of a circular cylinder. *Phys. Fluids* **31**, 2742–2744.

WILLIAMSON, C. H. K. 1989 Oblique and parallel modes of vortex shedding in the wake of a circular cylinder at low Reynolds numbers. *J. Fluid Mech.* **206**, 579–627.